Journal of Applied Fluid Mechanics, Vol. 10, No. 3, pp. 889-897, 2017.
Available online at www.jafmonline.net, ISSN 1735-3572, EISSN 1735-3645.
DOI: 10.18869/acadpub.jafm.73.240.25093

A Finite Volume Study on the Effects of Electro-Hydro-Dynamic Fluid Acceleration on Airflow Around a Cylinder at Low Reynolds Numbers

G. Tathiri[1†], H. Parishani[2] and E. Esmaeilzadeh[3]

[1]*Department of Engineering, Zanjan Branch, Islamic Azad University, Zanjan, Iran*
[2]*Department of Earth System Science, University of California Irvine, Irvine, CA 92697-3100, USA*
[3]*Department of Mechanical Engineering, University of Tabriz, Tabriz, Iran*

†*Corresponding Author Email: gh_tathiri@iauz.ac.ir*

(Received May 20, 2015; accepted January 17, 2017)

ABSTRACT

Applying a high-voltage electric field in a flow (electro-hydrodynamics or EHD) is a highly effective approach to locally accelerate a fluid to a desired speed. In this paper, a finite volume implementation is used to study the fluid flow around a fixed cylinder at a low Reynolds number. Two pairs of wire-plate electrodes are used to generate the electric field for fluid acceleration. Two Reynolds numbers are considered: Re=40, 100. We show that by increasing the Reynolds number, the relative effect of EHD is decreased. Further, we study the change in drag force due to EHD actuation. Finally, we showed that under certain voltage, electrode placement and Reynolds number the EHD fluid acceleration does not increase the total drag on the cylinder and yet leads to an increase in the total streamwise momentum transfer by augmenting the velocity at the top of the boundary layer.

Keywords: Drag force; Laminar boundary layer; Electro-hydro-dynamic fluid acceleration.

NOMENCLATURE

a	half distance between wire electrodes
c_P	pressure coefficient, dimensionless
D	cylinder diameter
D	electric displacement vector
E	electric field intensity
f	force
J	current density
k	conductivity
L	wire-plate horizontal distance
L_x	length of the channel
L_y	width of the channel
P	polarization vector
Re	Reynolds number, dimensionless
u	fluid velocity
U_∞, U_{inf}	free stream fluid velocity
V	potential field
Γ	diffusion coefficient
ε_0	permittivity of free space
μ_e	mobility of charged particles
ρ_e	electric charge density
ρ_f	fluid density
σ	electrical conductivity coefficient

1. INTRODUCTION

Flow and heat transfer control around a cylinder has been studied extensively by numerous researchers (Franke and Hogue 1991, Seyed-Yagoobi and Owsenek 1997; Seyed-Yagoobi and Bryan 1999; Lei *et al*. 2003; Artana *et al*. 2003, Sung *et al*. 2006, Tabatabaeian *et al*. 2012, Benard and Moreau 2013). Boundary layer manipulation leads to generation of additional turbulence and vortex shedding in the wake region, and hence is desirable for applications where an increased surface heat transfer is required. (Franke and Hogue 1991, Seyed-Yagoobi and Owsenek 1997; Seyed-Yagoobi and Bryan 1999; Bergles 1989; Bergles 1985; Yabe 1991). For this purpose, usually an increased momentum in the boundary layer leads to a higher drag force.

Methods of flow control may be divided into three categories (Bergles 1989; Bergles 1985): passive, active and compound control. Among the active flow control methods, Electro-Hydro-Dynamic (EHD) has received special attention. In this technique, a high voltage electric field is applied to accommodate a secondary flow and hence modify the momentum/energy flux locally as well as the downstream of the electrodes. The local modification is achieved through the collision of the migrating charged particles with the neutral species of the ambient medium. Therefore the EHD fluid

acceleration is highly desirable for controlled heat transfer and targeted cooling. (Bergles 1989; Bergles 1985; Yabe 1991; Leger *et al*. 2001; Owsenek 1993; Jewell-Larsen *et al*. 2006; Jewell-Larsen *et al*. 2009).

In practice, ionization is the result of applying a high potential difference between the two electrodes. The ions, which are affected by Coulomb force, transfer their momentum to the fluid particles (Leger *et al*. 2001) and consequently generate an accelerated flow (Fig. 1).

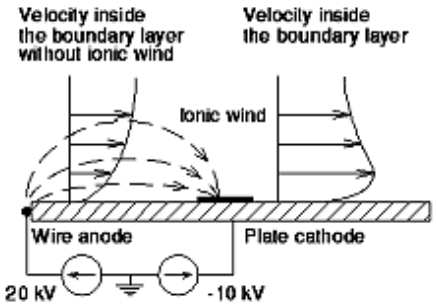

Fig. 1. Mechanism of ionic wind generation by applying electric field. After Leger *et al.* (2001) (Figure 2a therein).

Jewell-Larsen *et al*. (2006) studied the enhanced withdrawal of heat from microelectronic devices, focusing on design and optimization of electrostatic fluid accelerators for various wire-to-rod geometries. They concluded that one of the main challenges of practical electrostatic fluid accelerators is understanding of relative importance of design features. We note that by miniaturization of electronic devices, the relative importance of the design features may vary dramatically between structural integrity and heat withdrawal capabilities. The enhanced heat transfer is highly desirable and requires higher flow rates while the structural integrity of material limits that flow rate due to excessive drag, vibration/noise and corrosion. In another study, Jewell-Larsen *et al*. (2009) integrated an EHD cooling system to a laptop replacing the conventional fan blowers. They showed that the EHD cooling performs equally well in heat withdrawal and argued that with a minimal optimization, the EHD cooling performance can exceed that of a conventional fan cooling system.

In an experimental investigation, Hsu *et al*. (2007) studied the thermal performance of an EHD fluid accelerator at a miniaturized scale (O(100micron)). Their measurements showed that a 25ºC surface cooling is achievable over a heated surface. They applied a voltage of 8.5 kV and a current of 70 μA to achieve this cooling performance and argued that a better performance is achievable with a light optimization. Recently, in an excellent review, Wang *et al*. (2013) provided a comprehensive summary of the fluid-accelerator cooling methods specifically tailored for microelectronics. They argued that the electrostatic fluid accelerators show the highest heat-management gain on geometry with a small form factor.

So far, the studies concerning the enhanced heat transfer on the cylinders have not reported the drag consequences of the EHD fluid acceleration. The enhanced heat transfer is highly desirable but comes at a cost of increased drag. With the recent emergence of the miniaturized EHD fluid accelerators/actuators, understanding the flow pattern and the forces applied on the cooled object is essential for a highly specialized and efficient product design. Therefore, in this paper we focus on the effects of EHD-accelerated fluid on a cylinder at low Reynolds numbers. Namely, we investigate the boundary layer velocity profile and the resulted drag forces with and without EHD acceleration and the objective is to achieve a higher streamwise momentum transport with a minimal drag increase.

The first parts of this research focused on the fluid acceleration over a flat plate and around a NACA0024 airfoil and are recently published in Tathiri *et al*. (2014, 2016). The current paper extends those studies to a cylindrical geometry. The rest of the paper is organized as follows. Section 2 summarizes the methodology and algorithms and Section 3 deals with the results of deploying EHD fluid acceleration on a cylinder. Finally, Section 4 summarizes the results and conclusions.

2. METHODOLOGY

In this paper, the finite volume method is used to study the EHD fluid flow acceleration around a fixed cylinder at steady state. The geometry and domain of the problem is shown in Fig. 2. We report the results for L/D=2.5 in two cases of a/D=0.335, 0.835. Two Reynolds numbers of Re=40 and 100 (U_∞=0.012 and 0.03 m/s respectively) are studied for the applied voltages of 10, 15 and 20KV per case. This study is performed for D=4.8 mm while the center of the cylinder is located at x/D=6.6 and the wire electrodes are located at x/D=4. A summary of the boundary conditions is tabulated in Table 1.

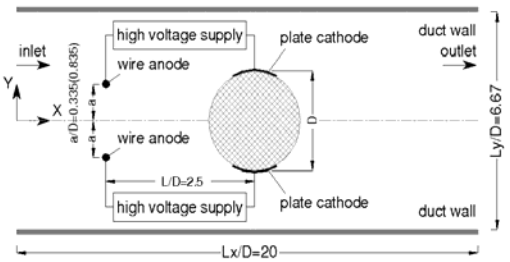

Fig. 2. Schematic geometry of the case study.

The problem is solved using the improved version of TEACH-2D program, originally developed by Gosman and Ideriah (1976). Quadratic elements are used in this study to mesh the computational domain.

Table 1 Summary of the boundary conditions

boundary	boundary conditions
flow inlet	velocity=const.
flow outlet	pressure=const.
top/bottom wall	zero gradient in y direction
cylinder surface	velocity=0 (no-slip condition)
wire/plate electrodes	electric potential =const. electric charge density=const.

In an EHD problem, governing equations of the fluid and electro-static fields are coupled. The electric field is governed by Maxwell's equations. From Gauss law we have:

$$\vec{\nabla} . \vec{D} = \rho_e, \tag{1}$$

where the electric displacement is:

$$\vec{D} = \varepsilon_0 \vec{E} + \vec{P}. \tag{2}$$

The electric field and polarization are described respectively as $\vec{E} = -\vec{\nabla} V$ and $\vec{P} = \varepsilon_0 (k-1)\vec{E}$. Therefore, the electric charge density can be calculated from conservation of the electric charge density using:

$$\vec{\nabla} . \vec{J} + \partial \rho_e / \partial t = 0. \tag{3}$$

As Melcher and Taylor (1995) have stated, this problem may be accurately modeled using ohmic conduction model and therefore the total current density in Eq. (3) is: $\vec{J} = \sigma \vec{E} + \rho_e \vec{u} + \rho_e \mu_e \vec{E}$. In this formulation, the terms on the right hand side represent the conduction, convection and ionic mobility, respectively. The convection and ionic mobility terms together represent the motion of a net electric charge in the fluid with velocity of $\vec{u}$ in an electric field of $\vec{E}$. The force applied to the molecules in the presence of an electric field consists of three parts:

$$\vec{f}_e = \rho_e \vec{E} - \frac{1}{2} E^2 \nabla \varepsilon + \frac{1}{2} \nabla \left[E^2 \rho (\frac{\partial \varepsilon}{\partial \rho}) \right]. \tag{4}$$

This formulation is derived by Melcher (1981) using a thermodynamic approach assuming that the polarization is a linear function of the applied electric field. The first term in the right hand of Eq. (4) is the Coulomb force and the last two are the polarization forces. For the purpose of this study, the polarization forces are negligible when compared to the Coulumb force. Therefore the last two terms can be safely neglected and thus the electric force can be approximated using $\vec{f}_e \cong \rho_e \vec{E}$. This assumption leads to decoupling of the hydrodynamic and the electrostatic equations in the solution procedure.

A steady and incompressible flow is considered for this study. The momentum and the energy equations may be written as:

$$\rho_f \vec{u} . \vec{\nabla} (\varphi) + \vec{V} . (\Gamma \vec{\nabla} \varphi) = S, \tag{5}$$

where ρ_f is the fluid density, $\vec{u}$ is the fluid velocity and Γ is the diffusion coefficient. The three terms in Eq. (5) are: convection, diffusion and source respectively. Now, the Poisson's and current continuity equations are:

$$\nabla . (\varepsilon_0 \nabla V) = -\rho \tag{6}$$

$$\varepsilon_0 \vec{E} . \nabla \rho = -\rho^2 \tag{7}$$

The finite volume method is applied to calculate the distributions of the electric potential and the space charge density. The derivatives in Eq. (6) can be discretized and evaluated from a piecewise-linear profile, with an integrated equation over the control volume as:

$$a_P V_P = a_E V_E + a_W V_W + a_N V_N + a_S V_S + b \tag{8}$$

where:

$$b = \frac{\rho_P}{\varepsilon_0}$$

$$a_P = a_E + a_W + a_N + a_S$$

$$a_{E,W} = \frac{1}{\Delta x (\delta x)_{E,W}} \quad , \quad a_{N,S} = \frac{1}{\Delta y (\delta y)_{N,S}}$$

and ρ_P is the spatial average of the charge density in the control volume. In this formulation, subscripts P, E, W, N and S represent the volume center, east, west, north and south respectively.

For the positive charge, the space charge density at each point is affected by the upstream and therefore, the upwind scheme can be applied to describe the space charge distribution for the positive corona. We note that in solving the Poisson equation, an elliptic mapping is performed to calculate the electric charge density and the voltages on a square inscribed in the cylinder. Integration of Eq. (8) over the control volume yields:

$$(E_x)_E A_E \rho_E - (E_x)_W A_W \rho_W + (E_y)_N A_N \rho_N - (E_y)_S A_S \rho_S = -\rho_P{}^2 \Delta \nu / \varepsilon_0 \tag{9}$$

where ρ_i is the value of ρ at the control volume face, A_i is the area of the control volume face and $\Delta \nu$ is the volume of the cell.

We followed the algorithm set forth by Lei *et al*. (2003) in calculating the space charge density based on the direction of the electric field and the sign of the space charge. Therefore, for the positive corona the upwind scheme is used yielding:

$$\rho_E = \begin{cases} \rho_p \to if (E_x)_E > 0 \\ \rho_E \to if (E_x)_E < 0 \end{cases} \tag{10}$$

The values of ρ_W, ρ_N, ρ_S are defined in a similar manner. Thus the coefficients of Eq. (8) can be determined as:

$$b = -\rho_P{}^2 \Delta V / \varepsilon_0$$

$$a_P = a_E + a_W + a_N + a_S + [(E_x)_E A_E - (E_x)_W A_W + (E_y)_N A_N - (E_y)_S A_S]$$

$$
\begin{aligned}
a_E &= \max[-(E_x)_E A_E, 0], \\
a_W &= \max[(E_x)_W A_W, 0], \\
a_N &= \max[-(E_y)_N A_N, 0], \\
a_S &= \max[(E_y)_S A_S, 0].
\end{aligned} \tag{11}
$$

For the negative charges, the downwind scheme is used (following Lei *et al*., 2003) to assure that the charge density at the interface is equal to that of the grid point on the downstream side.

In Fig. 3 the horizontal component of velocity in two sections of x/D=6.6 (on the center of the cylinder) and x/D=8.4 (downstream of the cylinder) are shown for three mesh setups. The maximum relative error between the two consecutive refinements decreases by refining the mesh and reaches <1% for 76800 in comparison with 19200 elements. Therefore convergence is achieved using 76800 elements (480 divisions in X and 160 divisions in Y direction).

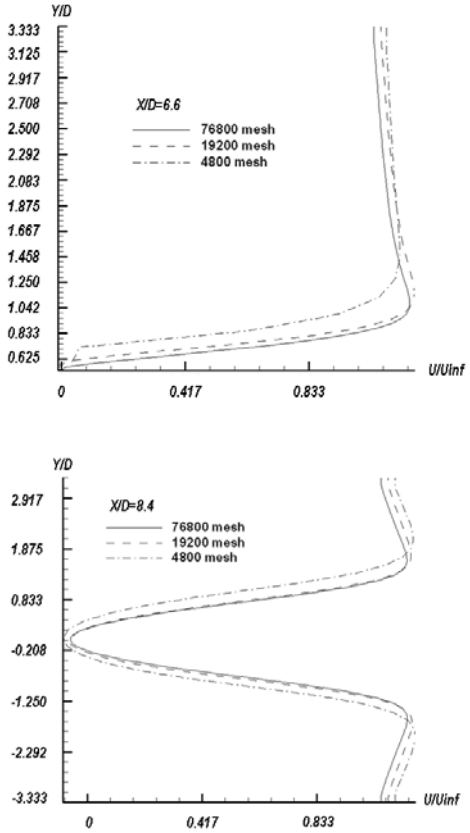

Fig. 3. The horizontal component of velocity at x/D=6.6 and x/D=8.4 (Re=40).

3. RESULTS

Fig. 4 shows the voltage and electric charge density fields of the two electrodes (computed individually and then superposed) for a/D=0.835. In a similar study by Lei *et al*. (2003), the electric density field is computed by superposition of the fields generated by four electrodes. Our Fig. 4(b) is in good agreement and is qualitatively comparable to Figs. 6 and 7 of Lei *et al*. (2003).

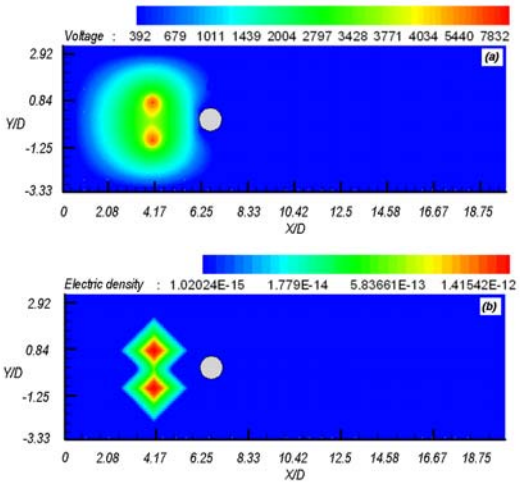

Fig. 4. Superposed (a) voltage field and (b) electric charge density of the electrodes. Both panels: a/D=0.835, ΔV=15 KV.

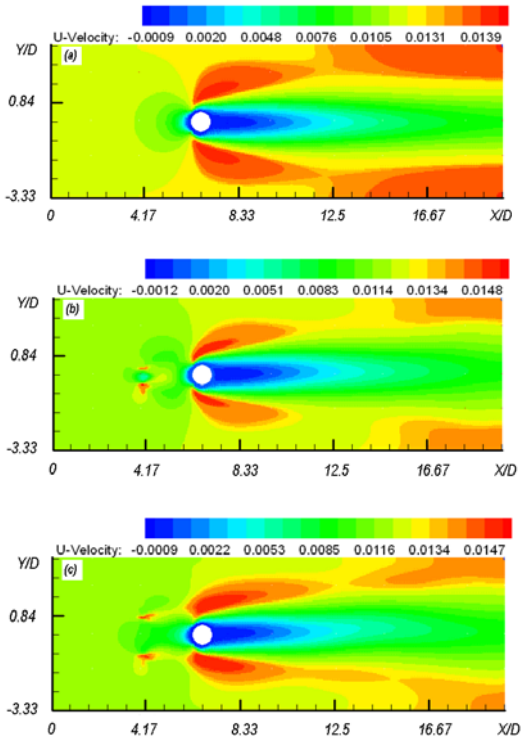

Fig. 5. Streamwise velocity contours at Re=40. (a) ΔV=0, (b) ΔV=15 KV, a/D=0.335, (c) ΔV=15 KV, a/D=0.835.

The streamwise velocity contours at ΔV=15 KV are shown in Fig. 5 and 6 for two Reynolds numbers of Re=40 and 100 respectively and compared with the case of ΔV=0. We observed that at both Reynolds numbers, the EHD fluid acceleration leads to a more localized velocity maxima in the boundary layer and also downstream in the wake region. However, the EHD effect on the flow pattern is more pronounced at Re=40. Also it is evident that the electrode placement of a/D=0.835 leads to a rise in the boundary layer height. This is clearly shown in Fig. 7 where the streamwise velocity profiles are compared at Re=40.

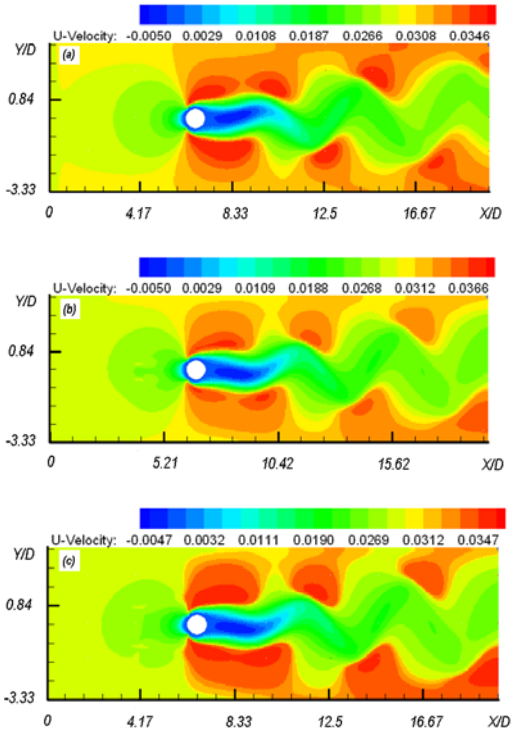

Fig. 6. Streamwise velocity contours at Re=100. (a) ΔV=0, (b) ΔV=15 KV, a/D=0.335, (c) ΔV=15 KV, a/D=0.835.

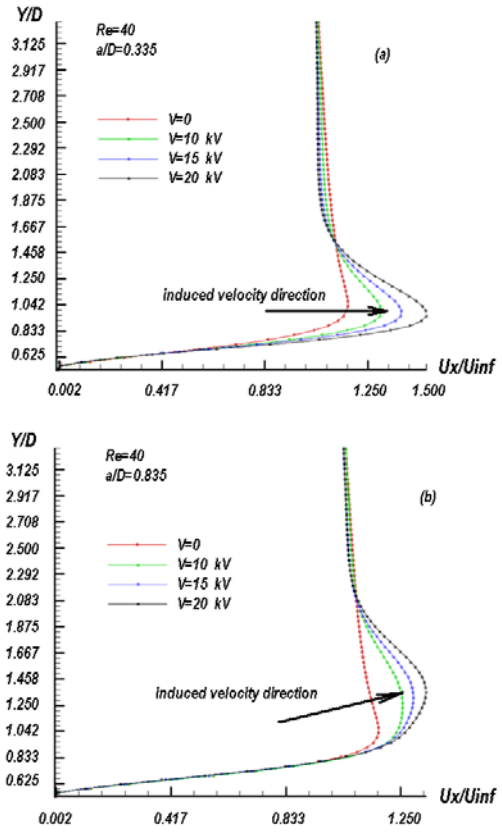

Fig. 7. Streamwise velocity in the top boundary layer of the cylinder at Re=40. (a) a/D=0.335, (b) a/D=0.835. The velocity maxima shift higher to the top of the boundary layer by increasing the applied voltage on panel (b).

The streamwise velocity in the top boundary layer at 90° angle is shown in Figs. 7 and 8 for different Reynolds numbers and arrangement of electrodes. In Fig. 7, we observe that the EHD application (ΔV=20 KV) at Re=40 yields a 17% increase in the maximum streamwise velocity. Furthermore, this high voltage field causes instability in the fluid flow after the cylinder. At Re=100, however, this increase is only ~2% (see Fig 8). The effects of applying electric field depend on the flow regime, applied voltage and placement of the electrodes. Thus, as expected, the EHD fluid acceleration is more effective at lower Reynolds numbers.

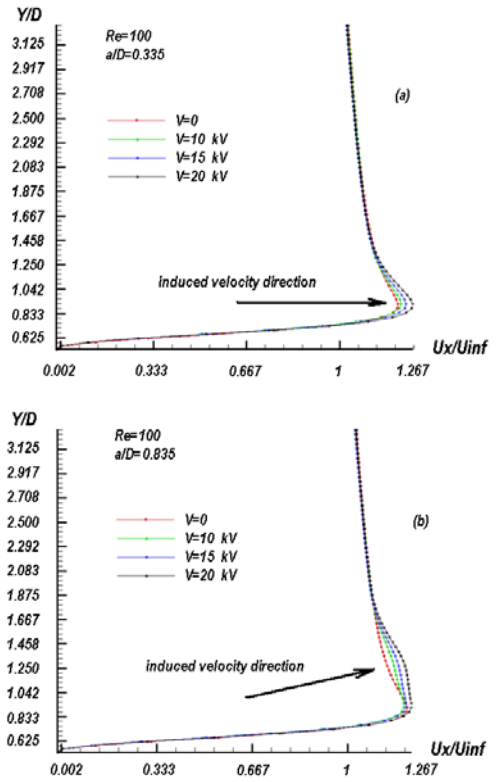

Fig. 8. Streamwise velocity in the top boundary layer of the cylinder at Re=100. (a) a/D=0.335, (b) a/D=0.835. The velocity maxima shift higher to the top of the boundary layer by increasing the applied voltage on panel (b). The shift is less significant when compared to Figure 7(b).

In the case of a/D=0.335, the streamwise velocity increase is observed to be closer to the surface of the cylinder (Fig 7a and 8a). Namely, the streamwise velocity maxima increases with the applied voltage at the same height inside the boundary layer. On the other hand, for a/D=0.835 the larger separation distance between the wire electrodes causes a velocity amplification further away from the surface and therefore leads to a thicker boundary layer (Fig 7b and 8b). In other words, for a/D=0.835 the streamwise velocity increase is accompanied by a shift away from the surface (shown by the arrows in Fig 7 and 8). At Re=100 (Fig 8), the changes in the boundary layer height and velocity maxima is similar in pattern but smaller than those of Re=40.

Next, the pressure coefficient is plotted in Fig. 9 for Re=40 and 100, with and without application of the electric field. The angle on the x-axis is measured from the stagnation point in front of the cylinder. For comparison we have shown the results of Artana *et al*. (2003) in the insets. Artana *et al*. (2003) measured the pressure coefficient at Re=21600 and 57600 for various applied voltages (currents). There are subtle differences between our results and measurements of Artana *et al*. (2003) in the immediate downstream of the wire-electrodes (up to ~40° angle). The reason for this difference is that Artana *et al*. (2003) used a single wire-electrode at the stagnation point while in our study we have two wire-electrodes well upstream of the cylinder stagnation point. Therefore the flow modification in Artana *et al*. (2003) is delayed to ~40° angle and further. Despite the fact that the Reynolds numbers in Artana *et al*. (2003) are about two orders of magnitude larger than those in this study, our results are in good qualitative agreement with the measurements of Artana *et al*. (2003) The flow modifications due to EHD is advected downstream of the cylinder. To better understand the flow modifications in the downstream, the velocity profiles in the horizontal mid plane of the channel at Re=40 and 100 are shown in Figs. 10 and 11.

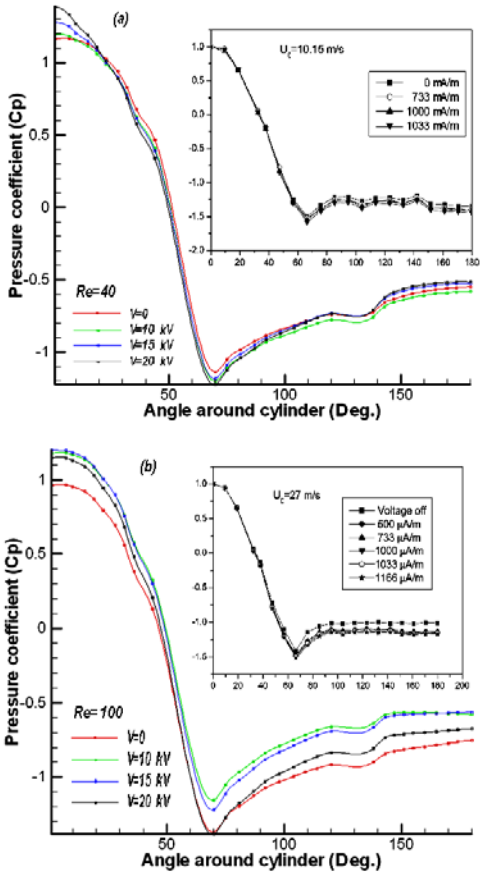

Fig. 9. The pressure coefficient (Cp) around the cylinder with different electric fields at (a) Re=40, (b) Re=100. The insets show the results of Artana *et al.* (2003) from their Figure 8a,b for Reynolds numbers of 21600 and 57600 respectively.

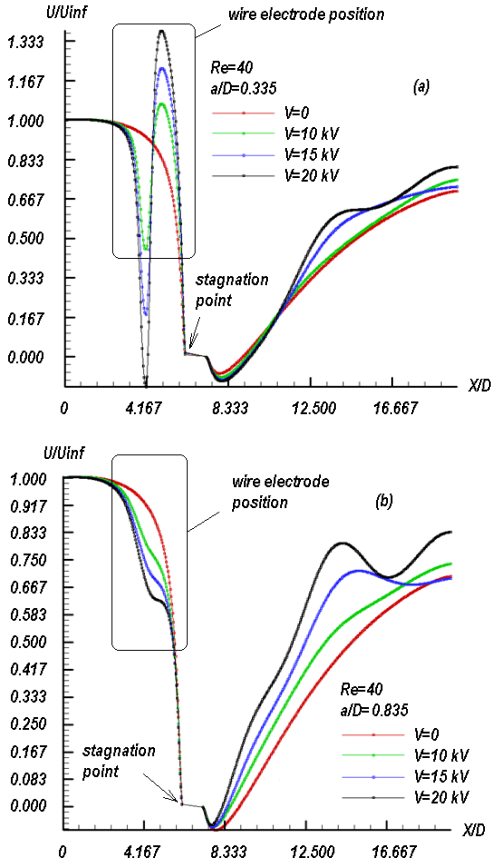

Fig. 10. Streamwise velocity profile in the horizontal mid plane of the channel at Re=40, (a) a/D=0.335, (b) a/D=0.835.

Figure 10 shows that at Re=40, the application of EHD increases the streamwise velocity downstream of the cylinder. Far from the electrodes, not only the velocity increases by voltage but also the flow becomes oscillatory and asymmetric (i.e. compare ΔV=20kV with ΔV=0 at both panels of Fig. 10). This oscillation is less significant in the close proximity of the electrodes. This shows a possibility of generating von Karman-like vortices using only the EHD fluid acceleration (ΔV=15kV and larger) in a flow where the von Karman vortices were essentially non-existent (ΔV=0). Indeed at a higher Reynolds number (Re=2500), using flow visualization, Artana *et al*. (2003) showed that applying an electric field leads to the formation of von Karman vortices and hence causes an asymmetric flow downstream of the cylinder (see Fig. 5a,b of Artana *et al*., 2003). The experimental realization and observation of this asymmetric pattern at low Reynolds numbers solely due to EHD fluid acceleration proves to be challenging. In this paper, however, we numerically show the asymmetry of the flow due to the EHD fluid acceleration at a low Reynolds number of Re=40. On the other hand in Fig. 11, we show that at Re=100 the effect of EHD on the flow downstream of the cylinder is less significant.

Furthermore, at Re=40 and in close placement of the electrodes (a/D=0.335), a significant flow reduction/reversal is observed at x/D~4.1 before the

flow impacts the cylinder. Continuing downstream, the flow is accelerated to a higher velocity than that of ΔV=0 right before stagnation (x/D~5). When the electrodes are far apart (Fig. 10b), the reduction in velocity is less significant (at x/D~4.1) and no velocity increase is observed before stagnation. In other words, close-placement of the electrodes causes the EHD energy to be dumped in the near field by increasing the kinetic energy of the fluid. In contrast, far-placement of the electrodes increases the flow energetics further downstream of the electrodes. At Re=100 (Fig. 11), the local effects of EHD is much less significant and are only limited to the alteration of the vortex shedding downstream of the cylinder.

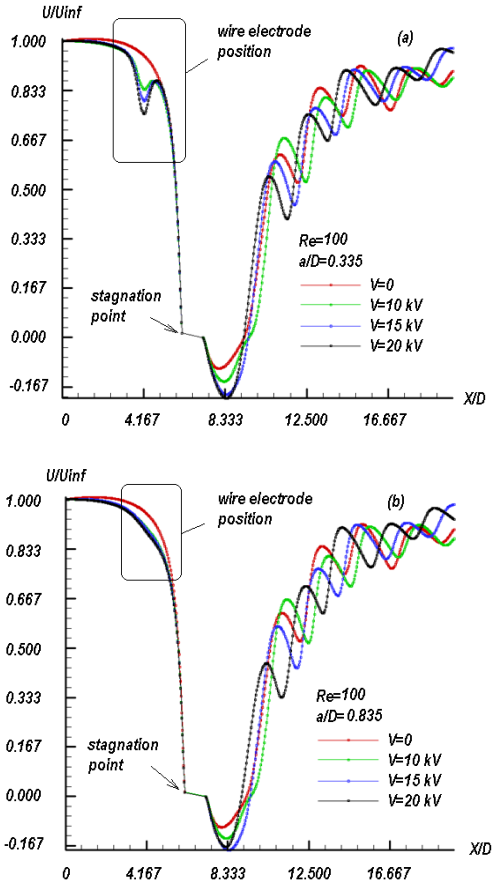

Fig. 11. Streamwise velocity profile in the horizontal mid plane of the canal at Re=100, (a) a/D=0.335, (b) a/D=0.835.

Finally, in the following the drag coefficients for different values of applied voltage and at two Reynolds numbers of Re=40 and 100 are tabulated and compared. The total drag is calculated using:

$$F_D = \int dF_x = \int P\cos\theta dA + \int \tau_w \sin\theta dA \qquad (12)$$

in which the first term in the right hand side is the pressure drag and the second term is the friction drag. θ is the angle between free stream velocity and the normal to the cylinder surface and τ_w is calculated by the velocity gradient on the cylinder surface. The results are presented for two different electrode arrangements (a/D=0.335 and a/D=0.835). Tables 2 and 3 show that at Re=40 the increase in drag coefficient is about 15-52% depending on the applied voltage. Also at Re=100 for a/D=0.335 a maximum of ~8.9% increase in the total drag is observed (Table 4). On the other hand, at Re=100 for a/D=0.835 we observed that the fluid acceleration leads to a slight reduction of the drag force (see Table 5). At Re=100 and a/D=0.835, the wide placement of the electrodes yields a thicker boundary layer and hence reduces the pressure and friction drags when compared to those of a/D=0.335. This clearly shows that the change in the drag force is highly dependent on the flow pattern and the placement of the wire electrodes. Namely, we showed the possibility of electrode arrangement (i.e. a/D=0.835 at Re=100) that does not increase the total drag on the cylinder by EHD fluid acceleration and yet leads to an increase in the total streamwise momentum by augmenting the streamwise velocity at the top of the boundary layer.

Table 2 Drag coefficient. Re=40, a/D=0.335

ΔV(KV)	*0*	*10*	*15*	*20*
Pressure drag	0.859	1.173	1.302	1.390
Friction drag	0.451	0.547	0.583	0.603
Total drag	1.310	1.720	1.885	1.993
increase%	-	31.3%	43.8%	52.1%

Table 3 Drag coefficient. Re=40, a/D=0.835

ΔV(KV)	*0*	*10*	*15*	*20*
Pressure drag	0.859	0.990	1.105	1.303
Friction drag	0.451	0.520	0.573	0.650
Total drag	1.310	1.509	1.678	1.953
increase%	-	15.2%	28.1%	49.0%

Table 4 Drag coefficient. Re=100, a/D=0.335

ΔV(KV)	*0*	*10*	*15*	*20*
Pressure drag	0.742	0.760	0.778	0.809
Friction drag	0.225	0.238	0.240	0.245
Total drag	0.968	0.997	1.018	1.054
increase%	-	3.1%	5.2%	8.9%

Table 5 Drag coefficient. Re=100, a/D=0.835

ΔV(KV)	*0*	*10*	*15*	*20*
Pressure drag	0.742	0.727	0.731	0.730
Friction drag	0.225	0.233	0.234	0.235
Total drag	0.968	0.960	0.965	0.965
increase%	-	-0.8%	-0.3%	-0.2%

4. CONCLUSION

In this paper, using a finite volume approach, we investigate the effects of EHD fluid acceleration on

the flow around a fixed cylinder. The fluid flow is solved for two Reynolds numbers of Re=40 and 100, once without an electric field and once with ΔV=10, 15 and 20 KV. Two pairs of wire and plate electrodes are used to accelerate the fluid. We observed that the placement/location of the electrodes is a highly important parameter in determining the pattern and extent of EHD effectiveness. Close-placement of the wire electrodes leads to an extensive local augmentation of the flow while the effects of far-placed electrodes show up further downstream of the cylinder. Taking advantage of this property, we were able to EHD-accelerate the fluid while keeping the total drag on the cylinder almost unchanged. We showed that electrode arrangement of a/D=0.835 at Re=100 leads to an increase in the streamwise momentum transfer by augmenting the streamwise velocity at the top of the boundary layer.

Consistent with the experimental results of Artana *et al*. (2003), we observed at Re=40 that the application of EHD causes the flow further downstream to become oscillatory and asymmetric. The flow asymmetry is generated using only the EHD fluid acceleration in a flow where the von Karman vortices were essentially non-existent. Finally we calculated and compared the drag coefficient in various settings. We show that the boundary layer fluid acceleration in general leads to a larger drag but it is feasible to find an arrangement of parameters (a/D=0.835 and Re=100 in this study) where the drag remains unchanged or is reduced slightly while the total streamwise momentum is increased by means of EHD fluid acceleration. This is a highly important finding for specialized applications where an increased streamwise momentum is desired with a minimal drag consequence.

REFERENCES

Artana, G., R. Sosa, E. Moreau and G. Touchard (2003). Control of the near-wake flow around a circular cylinder with electrohydrodynamic actuators. *Experiments in Fluids 35.*

Benard, N. and E. Moreau (2013). Response of a circular cylinder wake to a symmetric actuation by non-thermal plasma discharges. *Experiments in Fluids 54, 1467.*

Bergles, A. E. (1985). Techniques to augment heat transfer. *Handbook of Heat Transfer Applications (Edited by W. M. Rohsenow, J. P. Hartnett and E. N. Ganic), 2nd Edn. McGraw-Hill, New York.*

Bergles, A. E. (1989). The challenge of enhanced heat transfer with phase change. *Transe. VII Congresso Nazionale sulla Transmissione del Calore, Florence 1-12.*

Franke, M. E. and L. E. Hogue (1991, August). Electrostatic Cooling of a Horizontal Cylinder. *Transactions of the ASME 113.*

Gosman, A. D. and A. Ideriah (1976). TEACH-2E. *Tech. Rep. FM-83-2. University of California, Berkeley, Berkeley, CA.*

Hsu, C. P., N. E. Jewell-Larsen and I. A. Krichtafovitch, S. W. Montgomery, J. T. Dibene and A. V. Mamishev (2007). Miniaturization of Electrostatic Fluid Accelerators. *J. Microelectromech. Sys., 16, 4.*

Jewell-Larsen, N. E., H. Ran, Y. Zhang, M. K. Schwiebert and K. A. Honer Tessera (2009). *Electrohydrodynamic (EHD) Cooled Laptop. 25th IEEE SEMI-THERM Symposium.*

Jewell-Larsen, N. E., E. Tran, I. A. Krichtafovitch, and A. V. Mamishev (2006, February). Design and Optimization of Electrostatic Fluid Accelerators. *IEEE Transactions on Dielectrics and Electrical Insulation 13, 1.*

Leger, L., E. Moreau , G. Artana and G. Touchard (2001). Influence of a DC corona discharge on the airflow along an inclined flat plate. *Journal of Electrostatics 51-52, 300-306.*

Lei, H., L.-Z. Wang and Z. N. Wu (2003). Application of upwind and downwind schemes for calculating electrical conditions in a wire-plate electrostatic precipitator. *J. Comp. Phys. 193, 697-707.*

Melcher, J. R. (1981). Continuum electromechanics. *MIT Press.*

Melcher, J. R. and G. I. Taylor (1995). Electrohydrodynamics enhancement of heat transfer and fluid flow. *Recovery systems & CHP 15, no.5, 389-423.*

Owsenek, B. L. (1993). An experimental, theoretical and numerical investigation of corona wind heat transport enhancement. *M.Sc. thesis, Texas A&M University.*

Seyed-Yagoobi, J. and J. E. Bryan (1999). Enhancement of heat transfer and mass transport in single-phase and two-phase flows with electrohydrodynamics. *Advances in Heat Transfer 33.*

Seyed-Yagoobi, J. and B. L. Owsenek (1997). Theoretical and experimental study of electrohydrodynamic heat transfer enhancement through wire-plate corona discharge. *Journal of Heat Transfer 119.*

Sung, Y., W. Kim, M. G. Mungal and M. A. Cappelli (2006). Aerodynamic modification of flow over bluff objects by plasma actuation. *Experiments in Fluids 41, 479–486.*

Tabatabaeian, S., M. Mirzaei, A. Sadighzadeh, V. Damideh and A. Shadaram (2012). Experimental Investigation of the Effects of Various Plasma Actuator Configurations on Lift and Drag Coefficients of a Circular Cylinder Including the Effects of Electrodes. *Chinese Journal of Aeronautics 25, 311-324.*

Tathiri, Gh., H. Parishani, Gh. Pouryoussefi, E. Esmaeilzadeh, S. M. Mirsajedi, M. Mirzaei and N. Khatibzadeh (2016). Experimental investigation of separation control on a

NACA0024 airfoil using stationary and non-stationary AC-dielectric barrier discharge plasma actuator. *J. App. Fluid Mech., 9(2), 877-888.*

Tathiri, Gh., E. Esmaeilzadeh, S. M. Mirsajedi and H. Mahdavi Moghaddam (2014). Experimental Investigation of "Why an AC dielectric barrier discharge plasma actuator is preferred to DC corona wind actuator in boundary layer flow control? ". *J. App. Fluid Mech. 7(3), 525-534.*

Wang, H. C., N. E. Jewell Larsen and A. V. Mamishev (2013). Thermal management of microelectronics with electrostatic fluid accelerators. *App. Thermal Eng. 51, 190-211.*

Yabe, A. (1991). Active heat transfer enhancement by applying electric fields. *Proc. ASME/JSME Thermal Engineering Joint Conf. (Edited by J. R. Lloyd and Y. Kurosaki), pp. xv-xxiii.*